Exciton recombination and spin relaxation in strong magnetic fields in ultrathin (In,Al)As/AlAs quantum wells with indirect band gap and type-I band alignment

T. S. Shamirzaev,[1,2,3] J. Rautert,[4] D. R. Yakovlev,[4,5] and M. Bayer[4,5]

[1]*Rzhanov Institute of Semiconductor Physics, Siberian Branch of the Russian Academy of Sciences, 630090 Novosibirsk, Russia*

[2]*Ural Federal University, 620002 Yekaterinburg, Russia*

[3]*Laboratory of Advanced Materials Physics, Shpol'skii Theoretical Physics Chair, Moscow Pedagogical State University, 119435 Moscow, Russia*

[4]*Experimentelle Physik 2, Technische Universität Dortmund, 44227 Dortmund, Germany*

[5]*Ioffe Institute, Russian Academy of Sciences, 194021 St. Petersburg, Russia*

(Received 13 May 2021; accepted 30 June 2021; published 15 July 2021)

The exciton recombination and spin dynamics are studied in monolayer-thick (In,Al)As/AlAs quantum wells characterized by an indirect band gap and a type-I band alignment. The exciton recombination time and the photoluminescence intensity are strongly dependent on strength and orientation of an applied magnetic field. In contrast to no effect of an in-plane field, at a temperature of 1.8 K a magnetic field applied parallel to the growth axis drastically slows down the recombination and reduces the intensity of photoluminescence. The magnetic-field-induced circular polarization of photoluminescence is studied as a function of the magnetic field strength and direction, as well as sample temperature. The observed nonmonotonic behavior of these functions is provided by the interplay of bright and dark exciton states contributing to the emission. Taking into account the magnetic-field-induced redistribution of the indirect excitons between their bright and dark states, we evaluate the heavy-hole longitudinal g factor of 3.6, the radiative recombination time for the bright excitons of 0.13 ms, and the nonradiative recombination time of the bright and dark excitons of 0.43 ms, as well as the spin relaxation times of electron of 25 μs and heavy hole of 16 μs, bound in the exciton.

DOI: 10.1103/PhysRevB.104.045305

I. INTRODUCTION

At present, much attention is paid to the study of spin-dependent phenomena in semiconductor structures that could be interesting from the viewpoint of both basic physics and potential applications [1–3]. Since one of the key obstacles for spin-based quantum information processing is the spin relaxation, the search for objects with long spin lifetimes and their study are of great interest for spintronics and quantum information [4–8]. As it was shown theoretically, a slow down of the spin relaxation can be reached by carrier localization that suppresses the mechanisms determining the relaxation of freely moving particles [9,10]. The spin relaxation time of localized electrons can, indeed, reach milliseconds, as confirmed experimentally [11]. Therefore, to study localized exciton spin dynamics experimentally, it is necessary to use heterostructures with long exciton lifetimes. As we have shown recently, quantum wells (QWs) with an indirect band gap formed on the basis of III-V semiconductors [12–14] provide very long exciton lifetimes (up to milliseconds), so they can serve as model systems for these purposes [15–18].

The spin dynamics of localized excitons is related to the redistribution of exciton population between optically bright and dark states, and manifests itself in a magnetic-field-induced circular polarization [19]. It was studied recently in GaAs/AlAs QWs with an indirect band gap and a type-II band alignment [20,21]. However, the magnetic-field-induced polarization and the related spin dynamics of excitons in indirect band gap QWs with type-I band alignment have been weakly studied so far [18].

In this paper, we investigate the effects of a magnetic field on the exciton recombination and spin dynamics in ultrathin (In,Al)As/AlAs QWs with indirect band gap and type-I band alignment. The exciton photoluminescence (PL) intensity and the circular polarization degree (P_c) of the PL, induced by a magnetic field, show an unusual behavior. In the Voigt geometry, the magnetic field practically does not affect the PL, whereas in the Faraday geometry it induces a strong suppression of the PL intensity combined with an increase of the exciton recombination time. In tilted magnetic field, $|P_c|$ demonstrates a monotonic increase with saturation in high fields, whereas in the Faraday or close-to-Faraday geometry $|P_c|$ shows a nonmonotonic behavior as function of magnetic field. Namely, the modulus of the polarization degree increases in low magnetic fields until reaching a maximum, beyond which it decreases in strong fields. These experimental data are explained in the framework of a developed theoretical model [21–23], which takes into account the exciton distribution over the bright and dark states.

The paper is organized as follows. In Sec. II, the studied samples and the experimental techniques are described. In Sec. III we present the experimental data on the exciton dynamics obtained in external magnetic fields by time-integrated and time-resolved PL. Moreover, we present the

corresponding circular polarization degrees of PL, induced by the external magnetic field. In Sec. IV we compare the data to the model, based on the approach developed in our previous work [21,22], which allows us to evaluate the bright and dark exciton lifetimes, the carrier spin relaxation times, and the g factors. The conclusions are given in Sec. V.

II. EXPERIMENTAL DETAILS

The (In,Al)As/AlAs QW structure studied in this paper was grown by molecular-beam epitaxy on a semi-insulating (001)-oriented GaAs substrate in a Riber Compact system. The structure consists of an InAs QW layer embedded between 30-nm-thick barrier layers of AlAs, grown on top of a 200-nm-thick GaAs buffer layer [24]. The substrate temperature (T_S) during growth of the buffer and AlAs layers was 600 °C. The InAs QW layer was deposited with a nominal thickness of 1.4 monolayers (ML) at $T_S = 480$ °C with a rate of 0.04 ML per second, as calibrated in the center of the wafer using reference samples. To prevent InAs evaporation, the growth temperature was not increased during the deposition of a few initial monolayers of the second AlAs layer covering the QW. A 20-nm-thick GaAs cap layer protects the top AlAs layer against oxidation.

Commonly, thin QWs, for example in the GaAs/AlAs system [22], are described as thin slabs with abrupt heterointerfaces. However, the strong intermixing of the well and barrier materials for thin InAs QWs embedded in an AlAs matrix due to the strain-driven In segregation was directly demonstrated by scanning tunneling microscopy [25] and scanning transmission electron microscopy with visualization of the chemical elements distribution [26]. Thus the indium composition profile across the QW is not abrupt, but can be described using the phenomenological model of Muraki *et al.* [27]. Taking into account the amount of deposited InAs (N is the nominal thickness of InAs in monolayers) and the segregation coefficient of $R = 0.77$ for In in AlAs [25], we calculated the profile of the In concentration in the $In_xAl_{1-x}As$ alloy for a QW with $N = 1.4$ ML, as shown in Fig. 1(a). One can see that the peak In fraction x in the intermixed layer does not exceed 0.25.

The spatial profile of the band alignment calculated for this diffused QW in our previous study [17] is shown in Fig. 1(b). The structures have type-I band alignment with the lowest electron state belonging to the X_{xy} minimum of the QW conduction band. The indirect-in-momentum space band gap structure and the type-I band alignment of thin (In,Al)As/AlAs were experimentally confirmed in our recent study [26]. Additionally, it was determined that the characteristic (Urbach) energy tails in the state densities of electron and hole, formed due to fluctuations in QW thickness and alloy composition, are equal to 1.5 meV [26].

The sample was placed in a split-coil magnet cryostat and exposed to magnetic fields up to $B = 10$ T. The angle θ between the magnetic field direction and the QW growth axis (z axis) was varied between 0° (Faraday geometry) and 90° (Voigt geometry). For measurements in tilted geometry we fixed the magnetic field direction and rotated the sample. The emission was collected either in the direction along the field direction in the Faraday geometry for $0° \leqslant \theta \leqslant 45°$ or

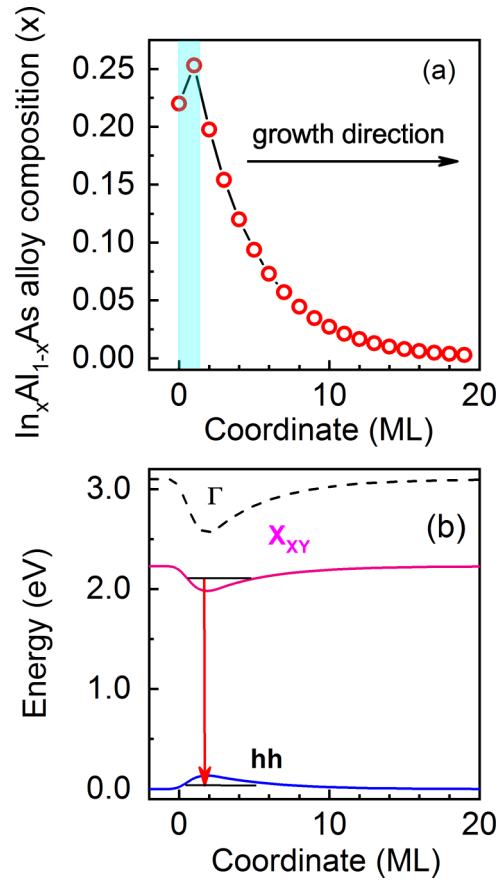

FIG. 1. (a) Segregation profile of In in a diffused (In,Al)As/AlAs QW with a nominal amount of deposited InAs of $N = 1.4$ ML (shown by cyan) along the QW growth axis, calculated according to Ref. [27]. (b) Band alignment of the diffused QWs along the growth direction. From top to bottom: Γ and X_{xy} conduction band minima and heavy-hole (hh) valence band levels. The red arrow marks the optical transition of the exciton to the ground state of the QW.

perpendicular to the field direction in the Voigt geometry for $45° \leqslant \theta \leqslant 90°$. The sample was in contact with pumped liquid helium or helium gas and its temperature was varied from $T = 1.8$ K up to 16 K. The PL was excited by the third harmonic of a Q-switched Nd:YVO_4 laser (3.49 eV) with a pulse duration of 5 ns. The pulse energy density was kept below 100 nJ/cm^2 and the pulse-repetition frequency was varied from 500 Hz up to 1 kHz [28]. The emitted light was dispersed by a 0.5-m monochromator. For the time-integrated measurements the photoluminescence was detected by a liquid-nitrogen-cooled charge-coupled-device (CCD) camera and for the time-resolved measurements a GaAs photomultiplier combined with a time-correlated photon-counting module was used. In order to monitor the PL decay in a wide temporal range of up to 1 ms, the time resolution of the detection system (i.e., the binning range of the photon counting events) was varied between 3.2 ns and 6.4 μs.

The exciton spin dynamics were analyzed from the PL by assessing the circular polarization degree P_c induced by the external magnetic field. P_c was evaluated from the PL data by

$$P_c = \frac{I_{\sigma^+} - I_{\sigma^-}}{I_{\sigma^+} + I_{\sigma^-}}, \tag{1}$$

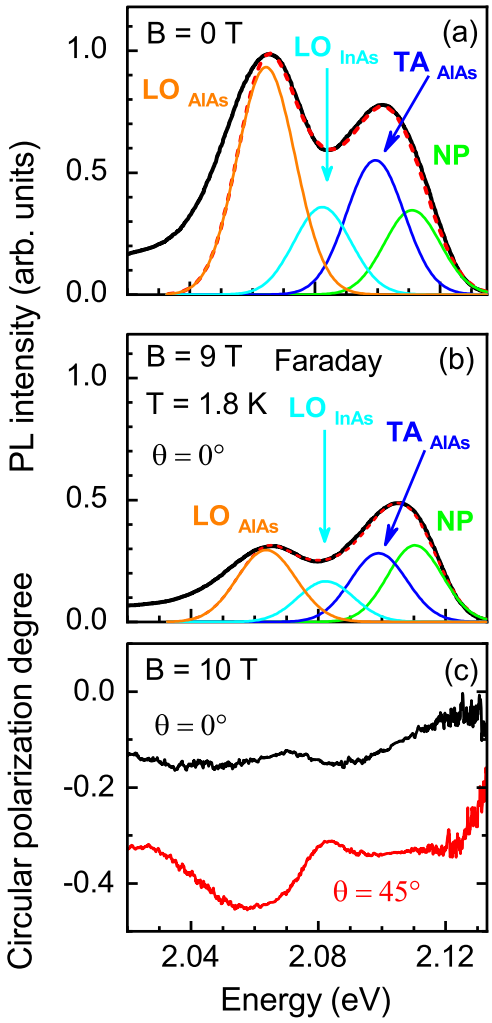

FIG. 2. Time-integrated PL spectrum of the ultrathin (In,Al)As/AlAs QW (black line) fitted with four Gaussian lines corresponding to the exciton recombination channels without and with involvement of phonons. The green, blue, cyan, and orange solid lines are the no-phonon line, the TA_{AlAs}, LO_{InAs}, and LO_{AlAs} phonon lines, respectively. The red dashed line is the fitted spectrum composed of the four lines. (a) $B = 0$ T and (b) $B = 9$ T for Faraday geometry. (c) Spectral dependence of the circular polarization degree of the PL induced by a longitudinal ($\theta = 0°$, black) and a tilted ($\theta = 45°$, red) magnetic field of 10 T.

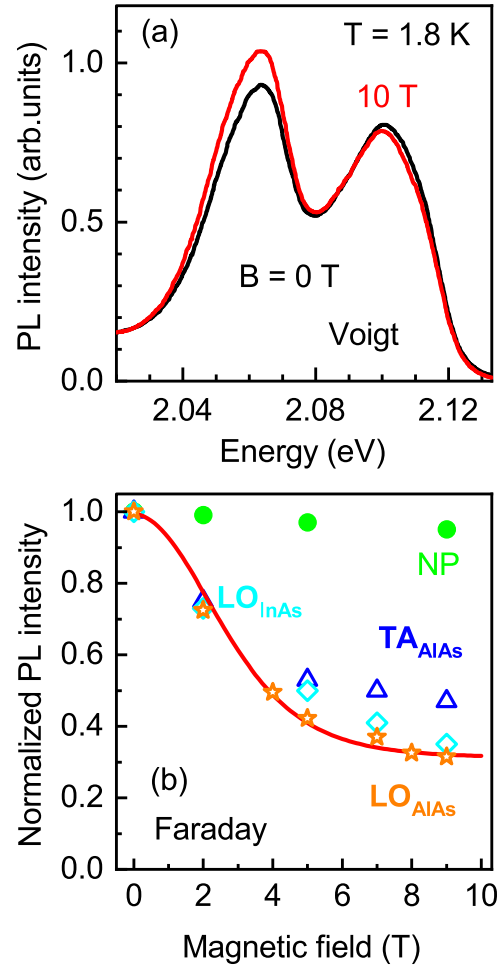

FIG. 3. Time-integrated PL spectra of the ultrathin (In,Al)As/AlAs QW measured in the Voigt geometry at different magnetic fields. (b) Normalized PL intensity of the NP line and the phonon-assisted lines as function of the magnetic field applied in the Faraday geometry. The solid line shows the results of a modeling for the LO_{AlAs} phonon-assisted emission line with the parameters given in Table I.

where I_{σ^+} and I_{σ^-} are the intensities of the σ^+ and σ^- polarized PL components, respectively. To determine the sign of P_c, we performed a control measurement on a diluted magnetic semiconductor structure with (Zn,Mn)Se/(Zn,Be)Se quantum wells, for which $P_c > 0$ in Faraday geometry [29].

III. EXPERIMENTAL RESULTS

A. Time-integrated photoluminescence

A time-integrated photoluminescence spectrum of the ultrathin (In,Al)As/AlAs QW at zero magnetic field is shown in Fig. 2(a) by the black line. The spectrum is contributed by several emission processes. It contains a no-phonon (NP) line and several lines of phonon-assisted recombination involving optical and acoustic phonons of InAs and AlAs. The lines associated with the transverse acoustic (TA) phonons of AlAs (12 meV) and the longitudinal optical (LO) phonons of InAs (25 meV) and AlAs (48 meV), all at the X point of the Brillouin zone [30], can be clearly identified. The lines are broadened due to the roughness of the QW interface [17,26]. An exemplary fit of the PL spectrum with four contributing Gaussian curves, each having the same width of 23 meV, is shown in Fig. 2(a) by the red dashed line. The energies of the phonon-assisted lines are shifted from the position of the NP line at 2.111 eV by the corresponding phonon energies. The deviation of the fitted spectrum from the experimental one in the low-energy region may result from two-phonon transitions that are not taken into account in the fitting procedure.

From Fig. 3(a) it is seen that in the Voigt geometry the magnetic field has very little effect on the photoluminescence intensity. However, in the Faraday geometry the PL intensity (I_{PL}) decreases strongly with increasing magnetic field strength, as one can see from comparing the spectra in

TABLE I. Parameters for the studied (In,Al)As/AlAs QW evaluated from the best fits to the experimental data. The parameters for a GaAs/AlAs QW, taken from Ref. [21], and a (Ga,Al)(Sb,As)/AlAs QW, taken from Ref. [18], are given for comparison.

Parameter	Value (In,Al)As/AlAs	Value GaAs/AlAs [21]	Value (Ga,Al)(Sb,As)/AlAs [18]	Comment
g_e	+2.0	+2.0	+2.0	[42,43]
$g_{hh\parallel}$	$+3.6 \pm 0.1$	$+3.5 \pm 0.1$	$+2.5 \pm 0.1$	Best fit
τ_r	0.13 ± 0.02 ms	0.34 ms	0.32 ms	Best fit
τ_{nr}	0.43 ± 0.02 ms	8.5 ms	2.1 ms	Best fit
τ_{sh}	16 ± 1 μs	3 ± 0.5 μs	30 ± 2 ns	Best fit
τ_{se}	25 ± 1 μs	33 ± 1 μs	100 ± 5 ns	Best fit
ξ	0.65 ± 0.05	0.75	0.25	Best fit
C_d	0.0015 ± 0.0002	0.001	0.002	Best fit

Figs. 2(a) and 2(b). Let us take a closer look at the magnetic field effects on the no-phonon and phonon-assisted emission lines. From fitting the PL spectra in magnetic field with the four Gaussian lines, see the examples in Figs. 2(a) and 2(b), the time-integrated intensities of these lines as functions of the longitudinal magnetic field are obtained, as shown in Fig. 3(b). Interestingly, the NP line and the phonon-assisted lines show very different behaviors. The intensity of the NP line is about constant; it decreases only by about 5% up to $B = 9$ T. By contrast, the intensities of the phonon-assisted lines are reduced by a factor of 3. The identification of the origin of the NP line has not been fully completed so far. A similar line was observed for ultrathin GaAs/AlAs QWs and possibly relates to emission from trions, i.e., charged excitons, each formed from a photogenerated electron-hole pair and a resident QW carrier [22]. Therefore, we exclude the NP line from the further analysis and will focus on the properties of the phonon-assisted lines.

B. Time-resolved photoluminescence

The photoluminescence dynamics measured for the NP, TA_{AlAs}, and LO_{AlAs} lines are shown in Fig. 4(a). At $T = 1.8$ K and $B = 0$ T the recombination occurs during two different stages: a fast nonexponential decrease during the first microsecond after the excitation pulse [presented in the inset of Fig. 4(a)], followed by an exponential decay with the time $\tau_{PL} = 0.21$ ms, which is the same for all PL lines. Since more than 95% of the intensity in the time-integrated spectra is collected in the time range exceeding one microsecond, we focus in our analysis on the long-term dynamics. All emission lines show similar changes in their dynamics with varying temperature, magnetic field, and sample orientation, so that we present and discuss below the typical behavior of the LO_{AlAs} line which is the strongest in intensity.

A magnetic field up to 10 T applied in the Voigt geometry does not affect the PL dynamics, as one can see in Fig. 4(b). On the contrary, strong changes are observed in the Faraday geometry. Here, the decay time increases from 0.21 ms to 0.45 ms with increasing magnetic field from 0 up to 10 T. The magnetic field dependence of the decay time is depicted in Fig. 5.

The integrated PL intensities measured at $B = 0$ T and 9 T at different temperatures are shown in Fig. 6. At zero magnetic field, the PL intensity, integrated over the LO_{AlAs} line, monotonically decreases by about one order of magnitude while the temperature increases from 2 K up to 15 K. This decrease is related to nonradiative centers at the heterointerfaces, which

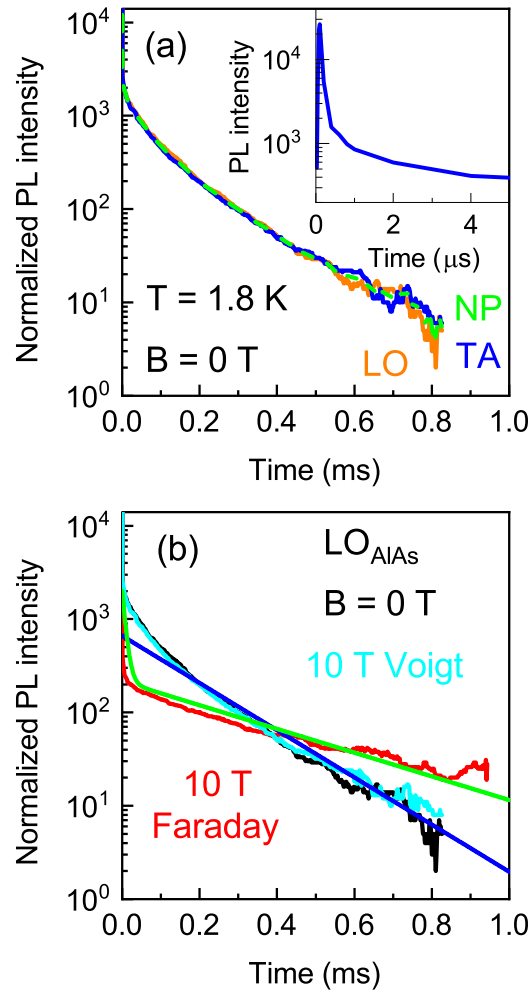

FIG. 4. (a) Decays of the NP (green), TA_{AlAs} (blue), and LO_{AlAs} (orange) PL components, measured at $B = 0$ T. The inset shows the initial time range up to 5 μs for the TA_{AlAs} component. (b) Dynamics recombination of the LO_{AlAs} emission line at $B = 0$ T (black) and 10 T in the Faraday (red) and Voigt (cyan) geometries. The blue and green solid lines are the results of modeling with the parameters given in Table I.

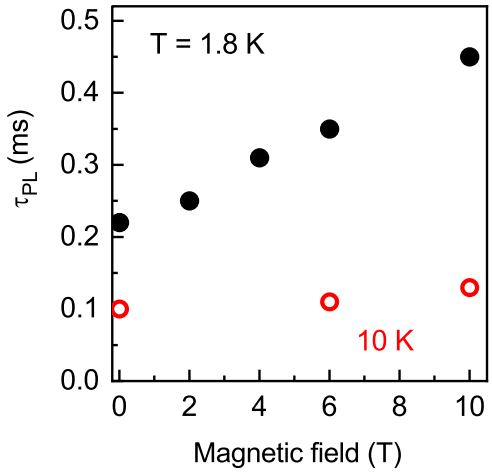

FIG. 5. PL decay time of the LO_{AlAs} line measured at $T = 1.8$ K (closed circles) and 10 K (open circles) as a function of magnetic field in the Faraday geometry.

capture excitons more efficiently at elevated temperatures, because the exciton diffusion length increases with increasing temperature [31,32].

In the Voigt geometry, an increase of the magnetic field up to 10 T has no effect on the temperature dependence of the PL intensity (not shown). For application of the magnetic field in the Faraday configuration, the temperature dependence changes drastically. The PL intensity increases by a factor of 2 with increasing temperature from 1.8 K up to 6 K (Fig. 6). It is surprising that such small changes in temperature result in a recovery of the PL intensity that was suppressed by the magnetic field in the Faraday geometry. A further temperature increase up to 15 K results in a monotonic decrease of the PL intensity.

The temperature increase leads to a recovery of the fast PL intensity decay in longitudinal magnetic field. One can see in Fig. 5 that already at $T = 10$ K the magnetic field dependence of τ_{PL} is nearly absent, while it is strong at 1.8 K.

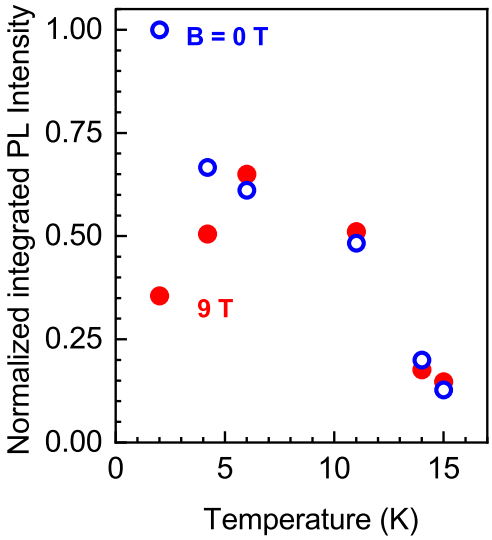

FIG. 6. Normalized intensity of the integrated PL of the LO_{AlAs} line as a function of temperature: $B = 0$ T (open circles) and $B = 9$ T (closed circles).

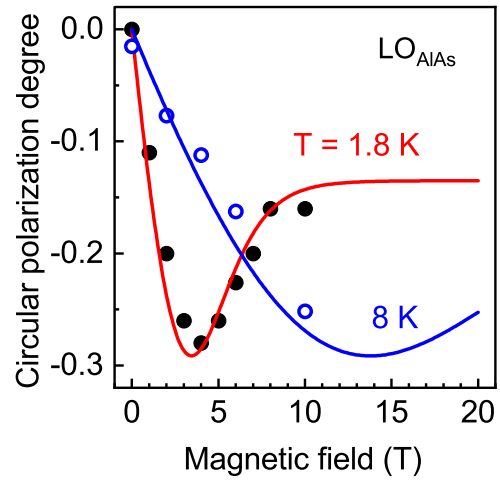

FIG. 7. Magnetic-field-induced circular polarization degree of the LO_{AlAs} line, measured at the temperatures of 1.8 (closed circles) and 8 K (open circles). The lines show the results of modeling with the parameters given in Table I.

C. Magnetic-field-induced circular polarization

The application of the magnetic field results in polarization of the emission, as shown in Fig. 2(c) for $B = 10$ T in the Faraday geometry $\theta = 0°$. One can see that P_c is negative (i.e., it is dominated by the σ^- polarized PL component) and varies spectrally. The absolute value of P_c is equal to 0.09 for the NP line and increases up to 0.14 and 0.15 for the TA_{AlAs} and LO_{AlAs} phonon-assisted lines, respectively.

The magnetic field dependencies of P_c measured at the maximum of the LO_{AlAs} line in the Faraday geometry for two different temperatures are shown in Fig. 7. The $P_c(B)$ at 1.8 K has an unusual nonmonotonic behavior. The modulus of the polarization degree increases in low magnetic fields, reaches a maximum absolute value, and then decreases in strong fields. The maximal value of the polarization degree, $|P_{c,\max}| = 0.29$, is achieved at $B = 3.8$ T. With increasing temperature the slope of the polarization rise decreases monotonically and the $|P_{c,\max}|$ value shifts towards stronger magnetic fields above 10 T.

For the longitudinal magnetic field fixed at 9 T, $P_c(T)$ demonstrates an unexpected nonmonotonic dependence, as shown in Fig. 8. $|P_c|$ increases from 0.15 up to 0.29 with increasing temperature from 1.8 up to 4.2 K. Then, it steadily decreases down to 0.095 with further temperature increase up to 14 K.

The $P_c(B)$ of the phonon-assisted lines depends strongly on the experimental geometry, as shown in Fig. 9. It behaves nonmonotonically in the Faraday geometry, while a finite angle θ between the magnetic field direction and the QW growth axis unexpectedly suppresses the decrease of $|P_c|$ in high magnetic fields. For a field tilt of $\theta = 45°$ $|P_c(B)|$ increases monotonically and saturates at 0.44 for 10 T.

To analyze the angular dependence of the polarization degree in more detail, we measured it at $T = 1.8$ K for $B = 4$

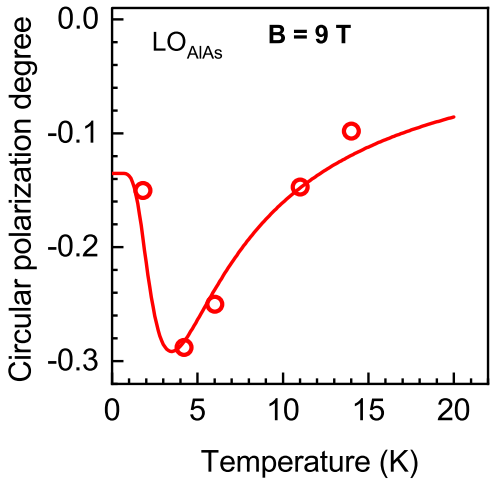

FIG. 8. Magnetic-field-induced circular polarization degree of the LO_{AlAs} line at $B = 9$ T as function of temperature. The circles are the experimental data. The line is the modeling result with the parameters given in Table I.

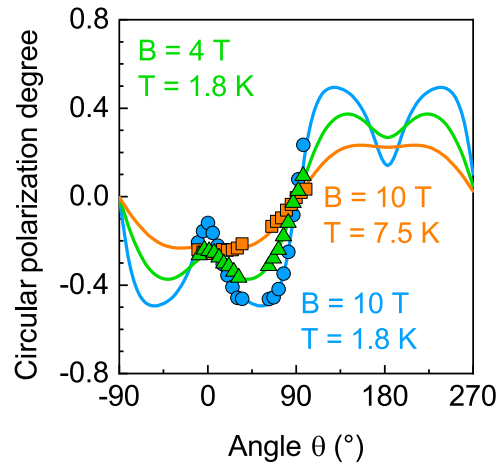

FIG. 10. Angle dependencies of $P_c(\theta)$ measured at $T = 1.8$ K for $B = 4$ T (green triangles) and 10 T (blue circles), and at $T = 7.5$ K for $B = 10$ T (orange squares). Lines show model calculation results with the parameters given in Table I.

and 10 T and at $T = 7.5$ K for $B = 10$ T. These results are shown in Fig. 10. One can see that $|P_c|$ increases for $0^\circ < \theta < 30^\circ$, changes insignificantly in the range of $30^\circ < \theta < 60^\circ$, and drops to zero for θ enlarged further towards 90°. For any magnetic field an increase of θ beyond 90° results in a change of the polarization sign; the PL is dominated then by the σ^+ polarized component. With increasing temperature up to 7.5 K at $B = 10$ T, the polarization $|P_c(\theta)|$ monotonically decreases when θ is varied from 0° to 90°.

The time evolution of P_c after pulsed excitation measured at $B = 8$ T is shown in Fig. 11. Its dynamics is unusually nonmonotonic. During the stage of the initial rise that is extended over 150 μs, P_c reaches -0.35 and then it tends to zero for time delays up to 1 ms. We need to note that the change in magnetic field strength results in a modification of the maximal value of the polarization degree only, while unexpectedly τ_s remains similar in the whole range of magnetic fields. Recently, we observed similar behavior of the spin relaxation times on magnetic field in ultrathin QWs GaAs/AlAs [21]. That is still an unclear but experimentally confirmed phenomenon since drastic magnetic-field dependence of the spin relaxation times was observed for electrons [11] and heavy holes [33] localized in Ga(In)As/GaAs and (In,Al)As/AlAs QDs, respectively. We hope that future studies on other thin indirect band gap QWs would help to resolve this ambiguity.

In conclusion of this section, we summarize the most important experimental findings as follows.

(i) The intensity and dynamics of the exciton radiative recombination depend strongly on the magnetic field strength in the Faraday and tilted-field geometries. This effect is absent

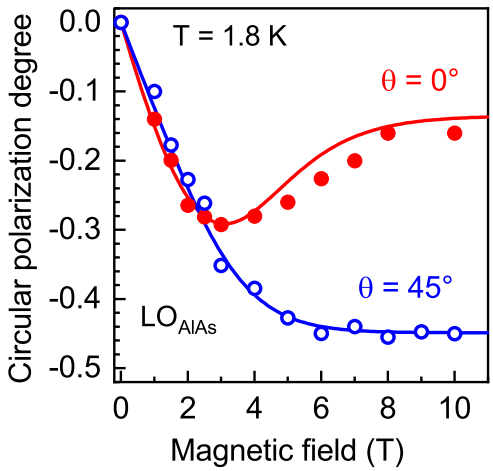

FIG. 9. Magnetic-field-induced circular polarization degree of the LO_{AlAs} line, in the longitudinal (closed red circles) and tilted by 45° (open blue circles) field configuration as function of the field strength. The lines are modeling results with the parameters given in Table I.

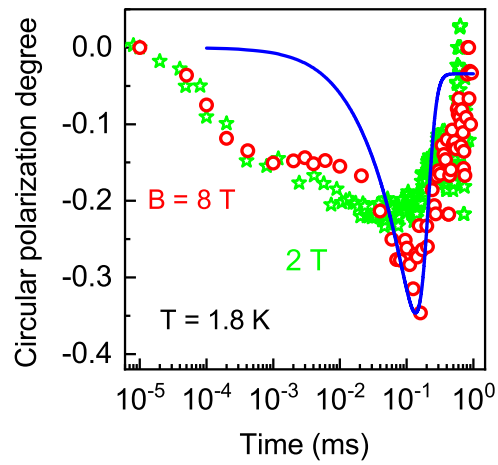

FIG. 11. Dynamics of the circular polarization degree of the LO_{AlAs} line measured at $T = 1.8$ K in the Faraday geometry for $B = 8$ T. The line shows model results with the parameters given in Table I.

in the Voigt geometry. Therefore, we conclude that it is caused by the magnetic field component parallel to the z axis.

(ii) A quite small temperature increase destroys the effect of the magnetic field on the exciton PL intensity and decay times. Thus we conclude that nonradiative recombination plays an important role for the exciton recombination dynamics in ultrathin (In,Al)As/AlAs QWs. Changes of the temperature or longitudinal component of the magnetic field can drastically affect the exciton distribution between the radiative and nonradiative recombination channels.

(iii) In the Faraday (and close-to-Faraday) geometry the absolute value of $|P_c|$ increases in low magnetic fields, but decreases in strong fields. However, in tilted magnetic field $|P_c(B)|$ demonstrates a monotonic increase with saturation in strong fields.

(iv) In the Voigt geometry the circular polarization degree $P_c(B) = 0$. Varying θ from 90° by a few degrees leads to a rapid increase of $|P_c|$.

(v) The temperature dependence of $|P_c|$ is also nonmonotonic. In high magnetic fields it increases with increasing temperature from 2 up to 4.2 K, and then it monotonically decreases with further temperature increase.

(vi) The dynamics of $|P_c|$ is strongly nonmonotonic in time. The $|P_c|$ is rising up to a maximum value during hundreds of microseconds and then drops down to zero.

IV. DISCUSSION

To explain the experimental findings we use the theoretical model developed in our recent papers [21,22]. The model accounts for the population and spin dynamics of the quartet of bright and dark exciton states. Below the main features of this model are presented. According to this model, an indirect-in-momentum space exciton in an (In,Al)As/AlAs QW with type-I band alignment is formed by a Γ-point heavy hole with angular momentum $j = 3/2$ and an electron with spin $s = 1/2$ in the X valley of the conduction band. Both carriers are localized within the (In,Al)As layer. The band diagram of the (In,Al)As/AlAs QW with indirect band gap and type-I band alignment along the growth direction z is shown schematically in Fig. 1(b).

The exciton fine structure multiplet consists of four states, after accounting for the angular momentum coupling of electron and hole. The two exciton states characterized by the angular momentum projections ±1 onto the z axis are bright and the two states with the projections ±2 are dark [21,22]. The bright excitons can emit light, while for the dark excitons radiative recombination is forbidden by the spin selection rule for optical transitions. The dark excitons recombine with a certain nonradiative decay rate, since phonon-assisted optical recombination of them is prohibited, as it was shown theoretically by Golub and Ivchenko [34] and experimentally in our recent study [5]. Thus dark excitons have a longer lifetime so that they can accumulate to form an exciton reservoir.

In a magnetic field the excitons undergo the Zeeman splitting, as shown schematically in Fig. 12. The hole eigenstates are still characterized by the z component of the angular momentum, $j_z = \pm 3/2$, and denoted in short by the state vectors $|\pm 3/2\rangle_z$. The electron eigenstates $|s\rangle_{\boldsymbol{B}}$ are characterized by the spin projection $s = \pm 1/2$ onto the (arbitrary) magnetic field direction. The exciton spin state is given by the product of the electron and heavy-hole eigenstates

$$|s j_z\rangle = |s\rangle_{\boldsymbol{B}} |j_z\rangle_z.$$

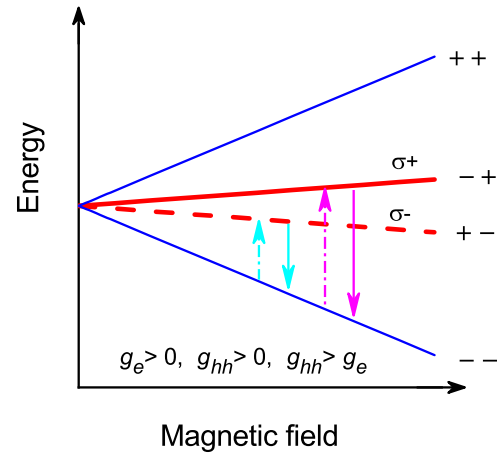

FIG. 12. Scheme of the exciton spin structure in a magnetic field, applied in the Faraday geometry, $\mathbf{B} \parallel z$. The blue lines show the optically dark (spin-forbidden) states. The red lines show the bright (spin-allowed) states that result in σ^+ (solid line) and σ^- (dashed line) polarized emission. The arrows indicate electron (hole) spin-flip processes increasing (dash-dotted) and decreasing (solid) the carrier's energy, respectively. For definiteness, the case of positive g_e and g_{hh} with $g_{hh} > g_e$, which provides an explanation of the main experimental findings, is shown. The definitions $++$, $--$, $-+$, and $+-$ correspond, respectively, to exciton states with spin projection $+2$, -2, $+1$, and -1. Note that the electron-hole exchange interaction in our indirect band gap structures is negligible, due to the weak overlap of the wave functions of the X electron and the Γ hole in momentum space, as it was shown theoretically [35,36] and experimentally [37,38].

The occupancies, f_{sj_z}, of the exciton Zeeman sublevels are controlled by the interplay between recombination processes and spin flips of either electron or hole, which provides exciton spin relaxation between its (Zeeman) sublevels. The occupancies can be described by a set of kinetic equations given in Ref. [21]:

$$\frac{df_{sj_z}}{dt} + (W_{\bar{s},s} + W_{\bar{j}_z,j_z}) f_{sj_z} - W_{s,\bar{s}} f_{\bar{s}j_z} - W_{j_z,\bar{j}_z} f_{s\bar{j}_z} + \mathcal{R} f_{sj_z} = G_{sj_z}. \tag{2}$$

Here $\bar{s} = -s$, $\bar{j}_z = -j_z$, and $W_{s,s'}$ (W_{j_z,j'_z}) are the electron (heavy-hole) spin-flip rates for the transitions $s' \to s$ ($j'_z \to j_z$), the operator $\mathcal{R}$ describes the radiative and nonradiative recombination of excitons, and G_{sj_z} is the exciton generation rate in the state $|s j_z\rangle$ [21].

The rates of the spin-flip transitions from the lower to higher and from the higher to lower Zeeman sublevels are different and can be interrelated as

$$W_{1/2,-1/2} = W_{-1/2,1/2} \exp\left(-\frac{g_e \mu_B B}{k_B T}\right),$$
$$W_{3/2,-3/2} = W_{-3/2,3/2} \exp\left(-\frac{g_{hh} \mu_B B_z}{k_B T}\right). \tag{3}$$

Here μ_B is the Bohr magneton, g_e and g_{hh} are the electron and heavy-hole Landé factors, B is the total magnetic field, and B_z is its z component. In the experiment, the Zeeman splittings can become comparable with the thermal energy, k_BT. In accordance with the notation of Ref. [21], $W_{-1/2,1/2} \equiv w_e$ and $W_{-3/2,3/2} \equiv w_h$.

In the frame of the model developed in Ref. [21], the exciton photoluminescence intensity and polarization are governed by the following set of parameters: (i) the values and signs of the electron and hole g factors (in combination with the strength and orientation of the magnetic field), (ii) the radiative (τ_r) and nonradiative (τ_{nr}) recombination times, the spin relaxation rates ($w_e = \tau_{se}^{-1}$, $w_h = \tau_{sh}^{-1}$, where τ_{se} and τ_{sh} are the spin relaxation times for electrons and heavy holes, respectively), describing the spin-flip rates for downward transitions, i.e., from an upper to a lower Zeeman sublevel, and (iii) the temperature, which determines the ratio of the upward and downward transitions.

A deviation of the optical selection rules that results in depolarization of the PL can be described in the following manner [21]:

$$P_c = \xi \frac{f_{+1} - f_{-1} + C_d(f_{-2} - f_{+2})}{f_{+1} + f_{-1} + C'_d(f_{-2} + f_{+2})}, \tag{4}$$

where $f_{\pm1}$ and $f_{\pm2}$ are the occupancies of the bright and dark exciton states, respectively, ξ is the depolarization factor, and the positive coefficients $C_d, C'_d \ll 1$ account for the emission of the dark states. Setting $\xi = 1$ and $C_d, C'_d = 0$, we come back to the strict selection rules, where exciton radiative recombination occurs via the bright states only. The parameters ξ and $C_d, C'_d \ll 1$ can depend on the phonon involved in the replica formation. For example, due to interface effects, the coupling of excitons to the short-wavelength phonons involved in the indirect photoemission can depend on the localization site (e.g., through the localization energy and, therefore, the localization length) and this dependence can be different for the TA and LO phonons. It is possible that spectral dependence of P_c [see Fig. 2(c)] is a result of difference in the heavy-light hole mixing strength that determines the PL depolarization factor ξ for the TA- and LO-assisted photoluminescence processes. In the following, for simplicity, we set $C_d = C'_d$. The details of the model to describe the recombination and spin dynamics of the excitons are presented in Ref. [21].

The model has a fair number of parameters. However, it was previously demonstrated that some of these parameters can be directly measured in experiment and others can be unequivocally evaluated from fits to various experimental dependencies [18,21,22]. Due to the large band gap at the X point, the spin-orbit contribution to the electron g factor is vanishingly small [39–41]. As a result, the electron g factor, g_e, is isotropic and its value almost coincides with the free-electron Landé factor of +2.0 [42,43]. The recombination times of the bright and dark excitons were unambiguously determined from the best fits to the PL intensity and PL decay at different temperatures and magnetic field strengths in the Faraday geometry (Figs. 4 and 8). Other parameters can also be obtained from the dependencies shown in Figs. 3, 7, 9, 10, and 11, similar to what has been done for GaAs/AlAs QWs [18,21]. These parameters from best fits that are shown in the corresponding figures are collected in Table I.

One can see that the experimental data can be well described by the model. Only for the dynamics of the circular polarization degree shown in Fig. 11 do we find a deviation between the calculation results and experimental data at the initial stage, while for the long-time range we have good agreement. This deviation can be corrected by suggesting a strong decrease of the hole spin relaxation time τ_{sh}. However, only a small deviation (about 10%) from the obtained values of τ_{sh} and τ_{se} abandons the fit quality of all dependencies presented in Figs. 3, 8, 9, and 10. Thus we suggest that the appearance of circular polarization at the initial stage of the PL decay is due to processes that are not taken into account in the used model. We observed a similar appearance of polarization at the initial stage of the PL decay upon nonresonant unpolarized excitation in a strong longitudinal magnetic field in structures containing (In,Al)As/AlAs QDs (unpublished). Probably, this effect is due to polarization during the process of energy relaxation of electrons and holes, or their spin-dependent capture into localized states of the QW. Clarifying the causes of this initial polarization is beyond the scope of this study.

It is interesting to compare the parameters obtained for the ultrathin (In,Al)As/AlAs QW with that for an ultrathin GaAs/AlAs QW [21] and (Ga,Al)(Sb,As)/AlAs QW [18]; see Table I. The values of the heavy-hole longitudinal g factors, as well as the bright exciton lifetime τ_r and the factor describing the radiative recombination of dark excitons C_d are close to each other in all systems.

We explain the decrease of the depolarization parameter ξ from 0.75 in GaAs/AlAs down to 0.65 in (In,Al)As/AlAs QWs by the increase of light-hole and heavy-hole mixing, caused by the increase of the alloy composition inhomogeneity in the (In,Al)As/AlAs QW. Indeed, the value of the depolarization parameter decreases drastically down to 0.25 in ultrathin indirect band gap (Ga,Al)(Sb,As)/AlAs QWs with strong fluctuations in composition and well width [18].

The light-hole and heavy-hole mixing leads to the appearance of linear polarization of the exciton emission in QWs under nonresonant excitation in zero magnetic field, as it was shown for various semiconductor heterostructures [23,44,45]. Linearly polarized PL components and the linear polarization degree of the exciton emission along the crystal axes $x \parallel [1\bar{1}0]$ and $y \parallel [110]$ are shown in Figs. 13(a) and 13(b), respectively. The emission is collected along the QW growth axis (z axis). The linear polarization degree, P_l, is evaluated from the data using the standard expression:

$$P_l = \frac{I_x - I_y}{I_x + I_y},$$

where I_x and I_y are the intensities of the PL components along the x and y axes. The emergence of intrinsic linear polarization confirms the light-hole and heavy-hole state mixing, implying a decreasing point symmetry of the studied structure that is induced by nonequivalent interfaces [23,46–48]. Since the difference between the upper and lower interfaces is stronger in the (In,Al)As/AlAs QW with In segregation [see Fig. 1(a)] than in the GaAs/AlAs QW, a smaller value of the

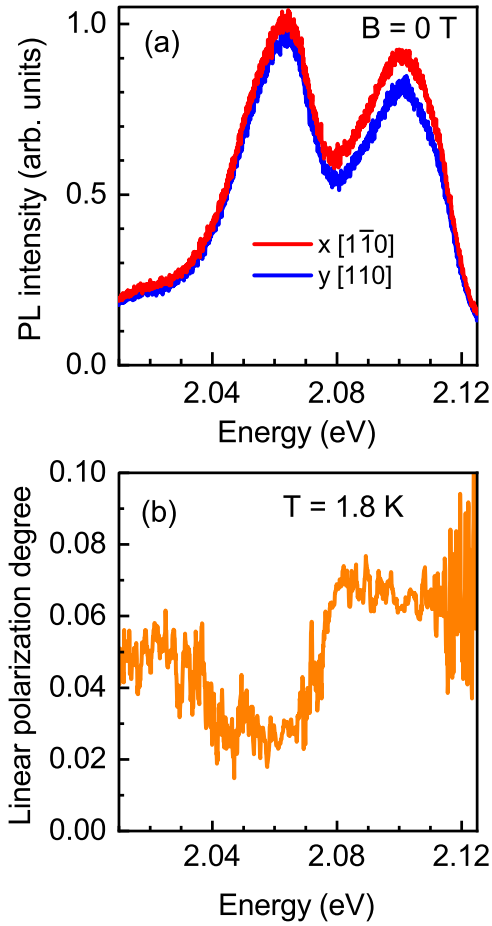

FIG. 13. (a) Linearly polarized PL components measured along the $x \parallel [1\bar{1}0]$ (red line) and $y \parallel [110]$ (blue line) crystal axes. (b) Linear polarization degree of the exciton emission along the crystal axes $x \parallel [1\bar{1}0]$ and $y \parallel [110]$ for a temperature of 1.8 K and at zero magnetic field.

depolarization factor (stronger depolarization of the PL) for (In,Al)As/AlAs QW seems reasonable.

Unexpected differences are, however, also observed in the parameter comparison as follows. (1) The recombination time of the dark exciton τ_{nr} decreases by a factor of 20 for (In,As)As/AlAs QW compared to that for the GaAs/AlAs QW and by a factor of 5 compared to that for the (Ga,Al)(Sb,As)/AlAs QW. (2) The heavy-hole spin relaxation time is surprisingly five times longer for the (In,As)As/AlAs QW than for the GaAs/AlAs QW, despite of a similar electron spin relaxation time in both systems.

The decrease of the dark exciton lifetime is due to a higher concentration of defects—centers of nonradiative recombination in the (In,Al)As/AlAs QWs. Indeed, the probability for the formation of such defects in A3B5 heterointerfaces increases with a decrease in diffusivity of adatoms on the growth surface, as was shown for different heterosystems: InAs/AlAs [49,50], InSb/AlAs [15,51], AlSb/AlAs [15], and GaAs/GaP [52]. Note that under similar growth conditions, the addition of indium atoms on the AlAs growth surface increases the adatoms diffusivity and improves the heterointerface quality [53]. However, we observe an increase of the nonradiative recombination rate in our structure and this feature is a result of the decrease in diffusion of the adatoms with a decrease of the temperature of epitaxial growth [49,50,54]. For the studied (In,Al)As/AlAs QW the growth temperature was 480 °C, which is by 120 °C lower than the 600 °C that was used for the GaAs/AlAs QWs growth in Ref. [22], and is 20 °C lower than the 500 °C used for (Ga,Al)(Sb,As)/AlAs QWs. The decrease in growth temperature of the (In,Al)As/AlAs QW was used to prevent desorption of In atoms and strong intermixing taking place at temperatures above 500 °C [50,55].

The second feature—the increase of the spin relaxation time of the heavy-hole—looks surprising. For (Ga,Al)(Sb,As)/AlAs QWs, with the same band structure leading to an indirect band gap and a type-I band alignment, τ_{sh} is about three orders of magnitude shorter and is equal to 30 ns. Moreover, our measurements of the heavy-hole spin relaxation time in (In,Al)As/AlAs QDs with the same band structure also show τ_{sh} shorter than 1 μs for fields larger than 8 T [33]. To clarify this difference in the heavy-hole spin relaxation times, additional studies are required.

V. CONCLUSION

The recombination and spin dynamics of excitons that are indirect in momentum space and involve electrons from the $X_{x,y}$ valleys were investigated experimentally in an ultrathin (In,Al)As/AlAs quantum well. In this system an indirect band gap and a type-I band alignment are realized. In longitudinal magnetic fields and at low temperatures, when the Zeeman splitting of the exciton levels exceeds the thermal energy $k_B T$, the relaxation from the bright to the dark exciton states results in a decrease of the exciton emission intensity, which is accompanied by an increase of the exciton recombination time. A recovery of the recombination time and the emission intensity is observed in the presence of a transverse magnetic field component, which mixes the dark and bright exciton states and for a temperature increase results in thermal population of the bright states. An unexpected feature obtained in this structure is the strong increase of the heavy-hole spin relaxation time. In order to clarify this feature we plan to extend our studies of long-lived localized excitons to other indirect band gap QWs based on A3B5 compounds.

ACKNOWLEDGMENTS

This work was supported by the Deutsche Forschungsgemeinschaft via Project No. 409810106 and by the Russian Foundation for Basic Research Grant No. 19-52-12001. M.B. acknowledges the support by the Deutsche Forschungsgemeinschaft-funded ICRC TRR 160. T.S.Sh. acknowledges the financial support by the Russian Foundation for Basic Research (Grant No. 19-02-00098) and support from the State Contract of the Moscow Pedagogical State University (MPGU) Physics of the perspective materials and nanostructures: basic researches and applications in material sciences, nanotechnologies and photonics supported by the Ministry of Education of the Russian Federation (AAAA-A20-120061890084-9) in collaboration with the Centre of collective usage Structural diagnostics of materials of the Federal Research Center RAS Crystallography and photonics.

[1] *Optical Generation and Control of Quantum Coherence in Semiconductor Nanostructures*, edited by G. Slavcheva and P. Roussignol (Springer-Verlag, Berlin, 2010).

[2] *Spin Physics in Semiconductors*, edited by M. I. Dyakonov (Springer, Berlin, 2008).

[3] N. Somaschi, V. Giesz, L. De Santis, J. C. Loredo, M. P. Almeida, G. Hornecker, S. L. Portalupi, T. Grange, C. Anton, J. Demory, C. Gomez, I. Sagnes, N. D. Lanzillotti-Kimura, A. Lemaitre, A. Auffeves, A. G. White, L. Lanco, and P. Senellart, Near-optimal single-photon sources in the solid state, Nat. Photon. **10**, 340 (2016).

[4] M. W. Wu, J. H. Jiang, and M. Q. Weng, Spin dynamics in semiconductors, Phys. Rep. **493**, 61 (2010).

[5] D. S. Smirnov, T. S. Shamirzaev, D. R. Yakovlev, and M. Bayer, Dynamic Polarization of Electron Spins Interacting with Nuclei in Semiconductor Nanostructures, Phys. Rev. Lett. **125**, 156801 (2020).

[6] A. Fert, The origin, development and future of spintronics, Phys. Usp. **51**, 1336 (2008).

[7] S. D. Bader and S. S. P. Parkin, Spintronics, Annu. Rev. Condens. Matter Phys. **1**, 71 (2010).

[8] M. S. Kuznetsova, J. Rautert, K. V. Kavokin, D. S. Smirnov, D. R. Yakovlev, A. K. Bakarov, A. K. Gutakovskii, T. S. Shamirzaev, and M. Bayer, Electron-nuclei interaction in X valley of (In, Al)As/AlAs quantum dots, Phys. Rev. B **101**, 075412 (2020).

[9] A. V. Khaetskii and Yu. V. Nazarov, Spin relaxation in semiconductor quantum dots, Phys. Rev. B **61**, 12639 (2000).

[10] A. V. Khaetskii and Y. V. Nazarov, Spin-flip transitions between Zeeman sublevels in semiconductor quantum dots, Phys. Rev. B **64**, 125316 (2001).

[11] M. Kroutvar, Y. Ducommun, D. Heiss, M. Bichler, D. Schuh, G. Abstreiter, and J. J. Finley, Optically programmable electron spin memory using semiconductor quantum dots, Nature (London) **432**, 81 (2004).

[12] M. E. Pistol and C. E. Pryor, Band structure of segmented semiconductor nanowires, Phys. Rev. B **80**, 035316 (2009).

[13] T. S. Shamirzaev, Type-I semiconductor heterostructures with an indirect gap conduction band, Semiconductors **45**, 96 (2011).

[14] D. S. Abramkin and T. S. Shamirzaev, Type-I indirect-gap semiconductor heterostructures on (110) substrates, Semiconductors **53**, 703 (2019).

[15] D. S. Abramkin, K. M. Rumynin, A. K. Bakarov, D. A. Kolotovkina, A. K. Gutakovskii, and T. S. Shamirzaev, Quantum dots formed in InSb/AlAs and AlSb/AlAs heterostructures, JETP Lett. **103**, 692 (2016).

[16] T. S. Shamirzaev, D. S. Abramkin, A. K. Gutakovskii, and M. A. Putyato, High quality relaxed GaAs quantum dots in GaP matrix, Appl. Phys. Lett. **97**, 023108 (2010).

[17] T. S. Shamirzaev, A. M. Gilinsky, A. K. Kalagin, A. V. Nenashev, and K. S. Zhuravlev, Energy spectrum and structure of thin pseudomorphic InAs quantum wells in an AlAs matrix: Photoluminescence spectra and band-structure calculations, Phys. Rev. B **76**, 155309 (2007).

[18] T. S. Shamirzaev, D. R. Yakovlev, A. K. Bakarov, N. E. Kopteva, D. Kudlacik, A. K. Gutakovskii, and M. Bayer, Recombination and spin dynamics of excitons in thin (Ga, Al)(Sb, As)/AlAs quantum wells with an indirect band gap and type-I band alignment, Phys. Rev. B **102**, 165423 (2020).

[19] E. L. Ivchenko, Magnetic circular polarization of exciton photoluminescence, Phys. Solid State **60**, 1514 (2018).

[20] T. S. Shamirzaev, Exciton recombination and spin dynamics in indirect-gap quantum wells and quantum dots, Phys. Solid State **60**, 1554 (2018).

[21] T. S. Shamirzaev, J. Rautert, D. R. Yakovlev, J. Debus, A. Yu. Gornov, M. M. Glazov, E. L. Ivchenko, and M. Bayer, Spin dynamics and magnetic field induced polarization of excitons in ultrathin GaAs/AlAs quantum wells with indirect band gap and type-II band alignment, Phys. Rev. B **96**, 035302 (2017).

[22] T. S. Shamirzaev, J. Debus, D. R. Yakovlev, M. M. Glazov, E. L. Ivchenko, and M. Bayer, Dynamics of exciton recombination in strong magnetic fields in ultrathin GaAs/AlAs quantum wells with indirect band gap and type-II band alignment, Phys. Rev. B **94**, 045411 (2016).

[23] T. S. Shamirzaev, J. Rautert, D. R. Yakovlev, M. M. Glazov, and M. Bayer, Intrinsic and magnetic-field-induced linear polarization of excitons in ultrathin indirect-gap type-II GaAs/AlAs quantum wells, Phys. Rev. B **99**, 155301 (2019).

[24] We choose for this study very thin (In, Al)As QWs in order to be able to compare their properties with another already studied model GaAs/AlAs QW structure, which has indirect band gap, but a type-II band alignment. Due to strain, high quality (In, Al)As/AlAs QWs can be grown of only a few monolayer thicknesses. This is not a crucial limitation for GaAs/AlAs heteropair; these structures can be grown with wider QWs.

[25] P. Offermans, P. M. Koenraad, R. Notzel, J. H. Wolter, and K. Pierz, Formation of InAs wetting layers studied by cross-sectional scanning tunneling microscopy, Appl. Phys. Lett. **87**, 111903 (2005).

[26] D. S. Abramkin, A. K. Gutakovskii, and T. S. Shamirzaev, Heterostructures with diffused interfaces: Luminescent technique for ascertainment of band alignment type, J. Appl. Phys. **123**, 115701 (2018).

[27] K. Muraki, S. Fukatsu, Y. Shiraki, and R. Ito, Surface segregation of In atoms during molecular beam epitaxy and its influence on the energy levels in InGaAs/GaAs quantum wells, Appl. Phys. Lett. **61**, 557 (1992).

[28] T. S. Shamirzaev, J. Debus, D. S. Abramkin, D. Dunker, D. R. Yakovlev, D. V. Dmitriev, A. K. Gutakovskii, L. S. Braginsky, K. S. Zhuravlev, and M. Bayer, Exciton recombination dynamics in an ensemble of (In, Al)As/AlAs quantum dots with indirect band-gap and type-I band alignment, Phys. Rev. B **84**, 155318 (2011).

[29] D. Keller, D. R. Yakovlev, B. König, W. Ossau, Th. Gruber, A. Waag, L. W. Molenkamp, and A. V. Scherbakov, Heating of the magnetic ion system in (Zn, Mn)Se/(Zn, Be)Se semimagnetic quantum wells by means of photoexcitation, Phys. Rev. B **65**, 035313 (2001).

[30] *Physics of Group IV Elements and III-V Compounds*, edited by O. Madelung, M. Schulz, and H. Weiss, Landolt-Börnstein Numerical Data and Relationships, New Series, Group III, Vol. 17, pt. a (Springer, Berlin, 1982).

[31] T. S. Shamirzaev, D. S. Abramkin, A. V. Nenashev, K. S. Zhuravlev, F. Trojanek, B. Dzurnak and P. Maly, Carrier dynamics in InAs/AlAs quantum dots: lack in carrier transfer from wetting layer to quantum dots, Nanotechnology **21**, 155703 (2010).

[32] I. N. Krivorotov, T. Chang, G. D. Gilliland, L. P. Fu, K. K. Bajaj, and D. J. Wolford, Exciton transport and nonradiative decay in semiconductor nanostructures, Phys. Rev. B **58**, 10687 (1998).

[33] D. Dunker, T. S. Shamirzaev, J. Debus, D. R. Yakovlev, K. S. Zhuravlev, and M. Bayer, Spin relaxation of negatively charged excitons in (In, Al)As/AlAs quantum dots with indirect band gap and type-I band alignment, Appl. Phys. Lett. **101**, 142108 (2012).

[34] L. E. Golub and E. L. Ivchenko, Spin-dependent phenomena in semiconductors in strong electric fields, New J. Phys. **15**, 125003 (2013).

[35] G. L. Bir and G. E. Pikus, *Symmetry and Strain-Induced Effects in Semiconductors* (Wiley, New York, 1974).

[36] G. E. Pikus and G. L. Bir, Exchange interaction in excitons in semiconductors, Zh. Eksp. Teor. Fiz. **60**, 195 (1971) [Sov. Phys. JETP **33**, 108 (1971)].

[37] J. Rautert, T. S. Shamirzaev, S. V. Nekrasov, D. R. Yakovlev, P. Klenovský, Yu. G. Kusrayev and M. Bayer, Optical orientation and alignment of excitons in direct and indirect band gap (In, Al)As/AlAs quantum dots with type-I alignment, Phys. Rev. B **99**, 195411 (2019).

[38] J. Rautert, M. V. Rakhlin, K. G. Belyaev, T. S. Shamirzaev, A. K. Bakarov, A. A. Toropov, I. S. Mukhin, D. R. Yakovlev, and M. Bayer, Anisotropic exchange splitting of excitons affected by Γ-X mixing in (In, Al)As/AlAs quantum dots: Microphotoluminescence and macrophotoluminescence measurements, Phys. Rev. B **100**, 205303 (2019).

[39] E. L. Ivchenko, *Optical Spectroscopy of Semiconductor Nanostructures* (Alpha Science, Harrow, UK, 2005).

[40] I. A. Yugova, A. Greilich, D. R. Yakovlev, A. A. Kiselev, M. Bayer, V. V. Petrov, Yu. K. Dolgikh, D. Reuter, and A. D. Wieck, Universal behavior of the electron g factor in GaAs/Al_xGa_{1-x}As quantum wells, Phys. Rev. B **75**, 245302 (2007).

[41] I. Vurgaftman, J. R. Meyer, and L. R. Ram-Mohan, Band parameters for III-V compound semiconductors and their alloys, J. Appl. Phys. **89**, 5815 (2001).

[42] J. Debus, T. S. Shamirzaev, D. Dunker, V. F. Sapega, E. L. Ivchenko, D. R. Yakovlev, A. I. Toropov, and M. Bayer, Spin-flip Raman scattering of the Γ-X mixed exciton in indirect band gap (In, Al)As/AlAs quantum dots, Phys. Rev. B **90**, 125431 (2014).

[43] V. Yu. Ivanov, T. S. Shamirzaev, D. R. Yakovlev, A. K. Gutakovskii, Ł. Owczarczyk, and M. Bayer, Optically detected magnetic resonance of photoexcited electrons in (In, Al)As/AlAs quantum dots with indirect band gap and type-I band alignment, Phys. Rev. B **97**, 245306 (2018).

[44] Yu. G. Kusrayev, A. V. Koudinov, I. G. Aksyanov, B. P. Zakharchenya, T. Wojtowicz, G. Karczewski, and J. Kossut, Extreme In-Plane Anisotropy of the Heavy-Hole g Factor in (001)-CdTe/CdMnTe Quantum Wells, Phys. Rev. Lett. **82**, 3176 (1999).

[45] E. L. Ivchenko and G. E. Pikus, *Superlattices and Other Heterostructures* (Springer, Berlin, 1997).

[46] G. E. Pikus and F. G. Pikus, The mechanism of heavy and light hole mixing in GaAs/AlAs superlattices, Solid State Commun. **89**, 319 (1994).

[47] E. L. Ivchenko, A. Yu. Kaminski, and U. Roessler, Heavy-light hole mixing at zinc-blende (001) interfaces under normal incidence, Phys. Rev. B **54**, 5852 (1996).

[48] M. M. Glazov, *Electron & Nuclear Spin Dynamics in Semiconductor Nanostructures* (Oxford University Press, Oxford, 2018).

[49] T. S. Shamirzaev, A. M. Gilinsky, A. K. Kalagin, A. I. Toropov, A. K. Gutakovskii, and K. S. Zhuravlev, Strong sensitivity of photoluminescence of InAs/AlAs quantum dots to defects: evidence for lateral inter-dot transport, Semicond. Sci. Technol. **21**, 527 (2006).

[50] T. S. Shamirzaev, A. V. Nenashev, A. K. Gutakovskii, A. K. Kalagin, and K. S. Zhuravlev, Atomic and energy structure of InAs/AlAs quantum dots, Phys. Rev. B **78**, 085323 (2008).

[51] D. S. Abramkin, A. K. Bakarov, M. A. Putyato, E. A. Emelyanov, D. A. Kolotovkina, A. K. Gutakovskii, and T. S. Shamirzaev, Formation of low-dimensional structures in InSb/AlAs heterosystem, Semiconductors **51**, 1233 (2017).

[52] D. S. Abramkin, M. A. Putyato, S. A. Budennyy, A. K. Gutakovskii, B. R. Semyagin, V. V. Preobrazhenskii, O. F. Kolomys, V. V. Strelchuk, and T. S. Shamirzaev, Atomic structure and energy spectrum of Ga(As, P)/GaP heterostructures, J. Appl. Phys. **112**, 083713 (2012).

[53] X. Z. Shang, W. C. Wang, S. D. Wu, Z. G. Xing, L. W. Guo, W. X. Wang, Q. Huang, and J. M. Zhou, Effects of indium doping on the properties of AlAs/GaAs quantum wells and inverted AlGaAs/GaAs two-dimensional electron gas, Semicond. Sci. Technol. **19**, 519 (2004).

[54] V. G. Dubrovskii, G. E. Cirlin, and V. M. Ustinov, Kinetics of the initial stage of coherent island formation in heteroepitaxial systems, Phys. Rev. B **68**, 075409 (2003).

[55] M. Schowalter, A. Rosenauer, D. Gerthsen, M. Arzberger, M. Bichler, and G. Abstreiter, Investigation of In segregation in InAs/AlAs quantum-well structures, Appl. Phys. Lett. **79**, 4426 (2001).